
E(2) Equivariant Neural Networks for Robust Galaxy Morphology Classification

Sneh Pandya^{*†}

Department of Physics
Northeastern University
NSF Institute for Artificial Intelligence and Fundamental Interactions
Boston, MA 02115

Purvik Patel^{*}

Khoury College of Computer Sciences
Northeastern University
Boston, MA 02115

Franco

Khoury College of Computer Sciences
Northeastern University
Boston, MA 02115

Jonathan Blazek

Department of Physics
Northeastern University
Boston, MA 02115

Abstract

We propose the use of group convolutional neural network architectures (GCNNs) equivariant to the 2D Euclidean group, $E(2)$, for the task of galaxy morphology classification by utilizing symmetries of the data present in galaxy images as an inductive bias in the architecture. We conduct robustness studies by introducing artificial perturbations via Poisson noise insertion and one-pixel adversarial attacks to simulate the effects of limited observational capabilities. We train, validate, and test GCNNs equivariant to discrete subgroups of $E(2)$ - the cyclic and dihedral groups of order N - on the Galaxy10 DECals dataset and find that GCNNs achieve higher classification accuracy and are consistently more robust than their non-equivariant counterparts, with an architecture equivariant to the group D_{16} achieving a $95.52 \pm 0.18\%$ test-set accuracy. We also find that the model loses $< 6\%$ accuracy on a 50%-noise dataset and all GCNNs are less susceptible to one-pixel perturbations than an identically constructed CNN. Our code is publicly available at <https://github.com/snehjp2/GCNNMorphology>.

1 Introduction

The study of galaxy morphology provides insight into how galaxies form and evolve over time. With the emergence of large-scale ground and space based observatories collecting massive amounts of data, deep learning has shown to be a promising candidate in its capabilities for powerful, efficient pattern recognition and inference across a variety of domains. Convolutional neural networks (CNNs) can be employed on the task of galaxy morphology classification [1–4] and be used to produce large galaxy morphological classification catalogues such as with the Dark Energy Survey Year 3 data [5].

^{*}equal contribution

[†]correspondence to pandya.sne@northeastern.edu

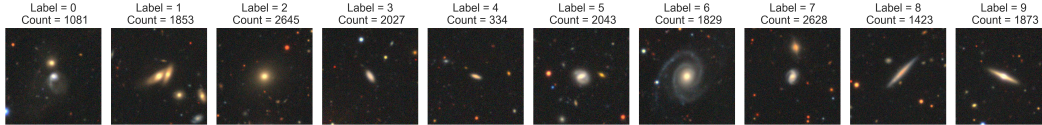


Figure 1: Examples of galaxy images and individual class abundances from the Galaxy10 DECals dataset containing 17, 736 labeled galaxies. Further information on each galaxy class can be found at <https://github.com/henrysky/Galaxy10>.

Group convolutional neural networks (GCNNs) [6] utilize symmetries of the data as an inductive bias in the architecture by using a higher degree of weight sharing compared to typical CNNs. [7, 8] further introduced "Steerable CNNs", allowing fast implementation of GCNNs equivariant to $E(2)$. CNNs endowed with symmetry priors were used for galaxy morphology classification in [9, 10].

The sensitivity of CNNs to adversarial perturbations has raised concerns about their practical deployment [11]. Quite (in)famously, the output of CNNs can be drastically altered by perturbing one pixel in the input image [12], and there exists a variety of attacks invisible to human perception that can cause misbehavior in CNNs [13]. This susceptibility to adversarial attacks has given rise to the study of robustness, wherein improvements in model training [14], data preprocessing [15], and architecture [16] have been studied. GCNNs robustness to geometric perturbations (e.g. rotations) were studied in [17]. [18, 19] studied the effects of adversarial perturbations on deep learning algorithms in astronomy and the effectiveness of domain adaptation techniques in mitigating such attacks.

In this paper, we construct GCNNs utilizing the symmetries of the 2D Euclidean group, $E(2)$, which contains all rotations, translations, and reflections in flat space for the task of galaxy morphology classification, exploiting the fact that there is no canonical orientation for galaxies and inferring their morphological properties. $E(2)$ encompasses both the cyclic (rotations) and dihedral groups (rotations and reflections), C_N and D_N , as discrete subgroups. We hypothesize that the robustness to symmetry transformations that are manifest in equivariant neural networks will result in increased robustness against adversarial perturbations that are relevant for the astronomical community.

2 Data & Method

2.1 Galaxy10DECals Dataset

The Galaxy10 DECals dataset [20] contains 17, 736 colored galaxy images (in g, r, and z band) of 10 distinct, imbalanced classes and is comprised of data from the Galaxy Zoo [21] Data Release 2 and DESI Legacy Imaging Surveys [22–24] as shown in Figure 1. The galaxy labels are a result of multiple rounds of rigorous volunteer votes and filtering. Each galaxy image is further equipped cosmological redshift; the sample of galaxies used here are primarily low-redshift ($z \sim 0.1$).

We apply normalization to take image pixel values from $[0, 255]$ to $[-1, 1]$, and uniformly apply data augmentation comprised of random rotations, translations, and center-crops during training to ensure non-equivariant models do not have an inherent disadvantage in experiments compared to equivariant ones [8]. Internal experiments tested the effectiveness of morphological opening as used in [3] and the inclusion of spectroscopic redshift, but found no benefit. We create a 20% test dataset of 3, 542 samples to evaluate the performance of our models, in which images are randomly rotated by an angle $\theta \in (0, 2\pi]$. We further conduct robustness studies by creating datasets with insertion of 25%, 50%, and 75% Poisson noise – as it closely resembles noise from CCD readouts or the atmosphere [19] – normalized with respect to the total original signal of the image. One-pixel attacks which simulate telescope processing errors were conducted using a differentiable genetic algorithm [12], in which a starting population of 400 agents is evolved over 200 generations to find pixel perturbations such that an image is misclassified by the model. One-pixel perturbations are a worst case scenario as a result of hardware failure at a detector level in an observational pipeline. These perturbations serve to test the out-of-distribution classification capabilities of our models in scenarios relevant to the astronomical community.

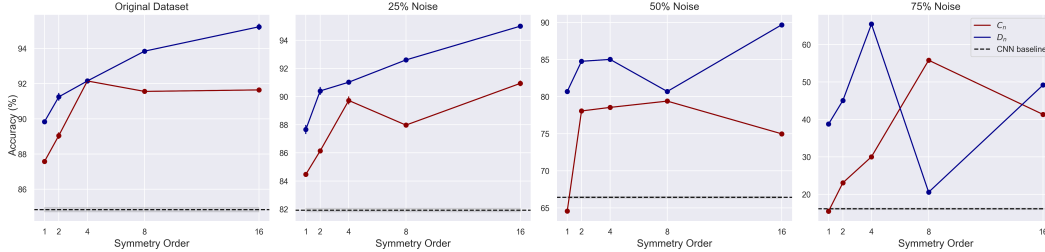


Figure 2: Model performance on test-set and noise experiments. C_N results are in red, D_N results in blue, and CNN baseline in black dashed-line. We see that equivariant models performance generally increases with N and continually outperforms the CNN baseline.

2.2 Architectures

We utilize the software package `escnn` [25, 26] to incorporate equivariance to all isometries of $E(2)$ [8] in constructing GCNNs equivariant to groups: $C_1, D_1^3, C_2, D_2, C_4, D_4, C_8, D_8, C_{16},$ and D_{16} as described at the end of § 1. Orders N higher than 16 were not studied due to being too computationally intensive. These networks construct specialized filters that are themselves equivariant to the desired symmetries, and therefore learn transformation-invariant features that preserve the underlying symmetries in the data throughout training. In this way, we ensure generalization over such transformations and their persistence in the presence of perturbations.

We construct deep GCNNs with 11 convolutional blocks containing a group-convolutional layer, batch-normalization, and ReLU activation [27]. Five intermittent pooling layers are used, which use point-wise average pooling for anti-aliased downsampling of feature maps. All features transform under the regular representation of the group, ρ_{reg} , with the hidden feature fields, i , including an expansion factor $f_i \in \{12, 24, 48, 48, 48, 48, 96, 96, 96, 112, 192\}$ to increase the number of convolutional channels. `GroupPooling` is used at the end to aggregate data across symmetry channels. The network lastly contains three fully-connected layers with ELU activation [28] for classification. Internal experiments were conducted to find optimal network depth. The effectiveness of dropout [29] and residual connections [30] was also studied, and no substantial improvement in results was found. The CNN baseline with an identical architecture (with the exception of no `GroupPooling`) is constructed in PyTorch [31] utilizing the non-equivariant counterparts of components mentioned previously. Models that are equivariant to $SO(2)$ and $O(2)$ were constructed; however, GCNNs that are equivariant to continuous groups cannot transform under ρ_{reg} and also require specific non-linearities [32]. This prevents the creation of an identical CNN baseline for comparison to these models. As such, their performance is not presented here.

3 Results

We trained all models using cross entropy loss, AdamW optimizer [33], and a step learning rate scheduler (10% decay at 25-epoch intervals for a starting $lr = 0.01$) for 100 epochs of training with early stopping on 4x NVIDIA A100-80GB GPUs. CNN training took $O(2)$ hours, while GCNN training took anywhere from $O(2)$ hours to $O(5)$ hours for higher-order GCNNs. Despite having less parameters, the training of GCNNs is more costly than CNNs due to the added expense of group convolution. GCNNs are believed to converge much more rapidly than CNNs [8], however this was not observed in our training. Classification uncertainties were obtained using bootstrap resampling.

3.1 Noise Experiments

On the original dataset, we find that all GCNNs outperform the CNN baseline, and the performance of GCNNs increases with the group order and inclusion of reflection symmetry. The D_{16} model achieves a $95.22 \pm 0.18\%$ accuracy, compared to the CNN with $84.84 \pm 0.14\%$ accuracy and outperforming the DenseNet in [3] by 6%. On the 25% and 50% noise datasets, the D_{16} model achieves a $95.00 \pm 0.18\%$ and $89.67 \pm 0.16\%$ accuracy, compared to $81.93 \pm 0.13\%$ and $66.43 \pm 0.13\%$ for the CNN baseline.

³We use the convention D_N (as opposed to the more common D_{2N}) for the dihedral group, following [8].

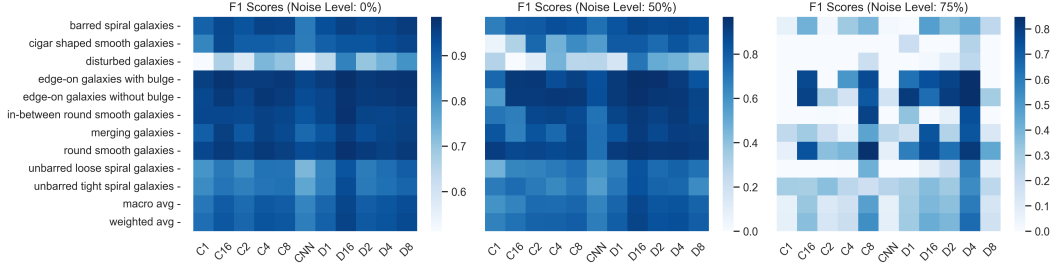


Figure 3: F1-score heatmaps for all models. We see that all models struggled to properly classify disturbed galaxies. It can be seen that in the presence of severe noise, the CNN struggles to properly classify all classes, while the best-performing D_4 model significantly struggles in three classes.

It is interesting to note that C_1 only contains the identity element, \mathbf{e} , and is therefore a trivial GCNN. Despite this, it still outperforms the CNN baseline in the original and 25% noise dataset which suggests the equivariance constraint, however minimal, is still providing some benefit over traditional convolution.

On the 75% noise dataset, we do not find strict performance benefits with increasing group order and symmetry. This can potentially be attributed to higher order GCNNs being more susceptible to symmetry breaking from the added perturbations; and as such the equivariance constraint of the model overpowers the expressivity as studied in [34–36]. The highest performing GCNN is the D_4 with $65.47 \pm 0.28\%$ accuracy, substantially outperforming the CNN baseline with $16.12 \pm 0.17\%$.

As shown in Figure 3, disturbed galaxies were the most difficult to classify for all models, likely due to their high variability in morphology and lack of persistent structure. There was also confusion between unbarred tight and loose spiral galaxies, which are also easy to confuse upon human evaluation. The similarity of the weighted and macro average F1-scores indicates that the class imbalance of the dataset did not have a significant effect. Figure 3 also illuminates that the success of the D_4 model in the 75% noise dataset was in its ability to classify unbarred and in-between round-smooth galaxies, which other GCNNs struggled to classify.

3.2 One-Pixel Attacks

We perform one-pixel adversarial attack experiments to simulate the effects of data processing noise sustained by image compression or telescope errors following the work of [19]. We apply the differentiable genetic algorithm to each image in the test set of 3,542 images for each model to see if a misclassification can be made within 200 evolutions of the population as discussed in § 2. The experiment was not able to be run on the D_{16} model due to inadequate computational resources.

Model	CNN	C_1	C_2	C_4	C_8	C_{16}	D_1	D_2	D_4	D_8	D_{16}
Incorrect (%)	3.60	3.60	1.90	1.90	2.35	3.15	2.20	1.75	2.05	2.31	N/A

The amount of images susceptible to one-pixel attacks from the genetic algorithm is less for GCNNs, however the previous expectation that GCNNs with higher order symmetries are more robust does not apply here as shown in the table. The lowest susceptibility was 1.75% of test-set images for the D_2 model. Susceptibility to one-pixel attacks is empirically ubiquitous, and their manifestations in astronomical settings are completely random. The results here communicate that within a reasonable search-space for a stochastic algorithm, one-pixel perturbations that can misclassify GCNNs are more sparse and more difficult to find, which suggest their increased robustness in a deployed setting.

4 Discussion & Future Work

We briefly analyze the models’ learned latent space using t-SNE [37]. As shown in Figure 4 (left), for one-pixel experiments, the expectation that increased robustness implies that images travel farther in latent space in order to cross a decision boundary (as seen in [19]) is not observed, as the D_2 model exhibits a mean traversed (Euclidean) distance less than the CNN. However, the mean distance for C_{16} - which is also more robust than the CNN - is twice as high as the CNN. It’s also seen in Figure 4

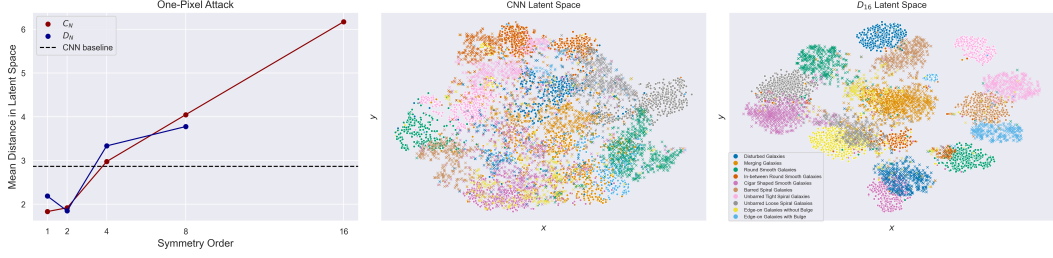


Figure 4: (Left) Mean Euclidean distance traversed in latent space for misclassified images in one-pixel experiments. (Middle / Right) t-SNE space constructions for CNN and D_{16} models for original (circle marker) and 50% noise (X marker) datasets. Latent space representations are the outputs of the model before the final fully connected layers.

(middle, right) that the D_{16} can better cluster galaxy classes in the 50% noise dataset and can therefore discern their properties better, but there is still significant movement and cluster-overlap in the latent space for some classes, which can explain the drop in accuracy seen in Figure 2. The significance of these effects increase with the amount of noise added, and can be mitigated in networks trained with domain adaptation [19]. The CNN movement in latent space is overall less, however the decision boundaries are significantly more ill-defined which can explain the model’s lack of robustness. In the future, it would be beneficial to conduct a more extensive analysis on the learned representations of GCNNs to interpret their increased robustness on this task.

Our work suggests that GCNNs are more robust than typical CNNs against adversarial perturbations that are common in astronomical imaging pipelines. Our models are able to perform with minimal data preprocessing to correct the class imbalance in our datasets or enhance the central galactic structure. In the future, the inclusion of domain adaptation in training and spectroscopic redshift as a feature may improve robustness. It would also be interesting to study robustness with respect to high redshift galaxies and dim low-redshift galaxies which are noisier and fainter than the sample of galaxies used here. The application of equivariant models has the potential to enhance the classification of over 20 billion galaxies from the Legacy Survey of Space and Time (LSST) at the Vera Rubin Observatory [38], deepening insights into their formation and evolution.

5 Broader Impacts

The techniques presented here have the potential to classify and extract features from images of arbitrary orientation and of significantly degraded quality, and as such warrant ethical concerns for maladaptations of this work. The exploitation of computer vision technologies for uses of surveillance is a poison. The authors steadfastly abhor the use of deep learning for purposes that do not seek to further scientific knowledge or provide a beneficial and equitable service to society.

6 Acknowledgments and Disclosure of Funding

We thank the anonymous referees for their useful comments. SP acknowledges support from the National Science Foundation under Cooperative Agreement PHY- 2019786 (The NSF AI Institute for Artificial Intelligence and Fundamental Interactions, <https://iaifi.org>). SP, PP, and FO acknowledge support from graduate teaching assistantships at Northeastern University. We thank Aleksandra Ćiprijanović at Fermilab for her useful comments on this work, and Robin Walters at Northeastern University for introducing us to equivariance. Computations were run on the FASRC Cannon cluster supported by the FAS Division of Science Research Computing Group at Harvard University.

References

- [1] A. K. Aniyan and K. Thorat. Classifying radio galaxies with the convolutional neural network. *The Astrophysical Journal Supplement Series*, 230(2):20, jun 2017. doi: 10.3847/1538-4365/aa7333. URL <https://dx.doi.org/10.3847/1538-4365/aa7333>.
- [2] V Lukic, M Brüggén, J K Banfield, O I Wong, L Rudnick, R P Norris, and B Simmons. Radio galaxy zoo: compact and extended radio source classification with deep learning. *Monthly Notices of the Royal Astronomical Society*, 476(1):246–260, jan 2018. doi: 10.1093/mnras/sty163. URL <https://doi.org/10.1093/mnras/sty163>.
- [3] Wuyu Hui, Zheng Robert Jia, Hansheng Li, and Zijian Wang. Galaxy morphology classification with densenet. *Journal of Physics: Conference Series*, 2402(1):012009, dec 2022. doi: 10.1088/1742-6596/2402/1/012009. URL <https://dx.doi.org/10.1088/1742-6596/2402/1/012009>.
- [4] Anna MM Scaife and Fiona Porter. Fanaroff–riley classification of radio galaxies using group-equivariant convolutional neural networks. *Monthly Notices of the Royal Astronomical Society*, 503(2):2369–2379, 2021.
- [5] Ting-Yun Cheng, Christopher J Conselice, Alfonso Aragón-Salamanca, M Agüena, S Allam, F Andrade-Oliveira, J Annis, A F L Bluck, D Brooks, D L Burke, M Carrasco Kind, J Carretero, A Choi, M Costanzi, L N da Costa, M E S Pereira, J De Vicente, H T Diehl, A Drlica-Wagner, K Eckert, S Everett, A E Evrard, I Ferrero, P Fosalba, J Frieman, J García-Bellido, D W Gerdes, T Giannantonio, D Gruen, R A Gruendl, J Gschwend, G Gutierrez, S R Hinton, D L Hollowood, K Honscheid, D J James, E Krause, K Kuehn, N Kuropatkin, O Lahav, M A G Maia, M March, F Menanteau, R Miquel, R Morgan, F Paz-Chinchón, A Pieres, A A Plazas Malagón, A Roodman, E Sanchez, V Scarpine, S Serrano, I Sevilla-Noarbe, M Smith, M Soares-Santos, E Suchyta, M E C Swanson, G Tarle, D Thomas, and C To. Galaxy morphological classification catalogue of the dark energy survey year 3 data with convolutional neural networks. *Monthly Notices of the Royal Astronomical Society*, 507(3):4425–4444, jul 2021. doi: 10.1093/mnras/stab2142. URL <https://doi.org/10.1093/mnras/stab2142>.
- [6] Taco S. Cohen and Max Welling. Group equivariant convolutional networks, 2016.
- [7] Taco S. Cohen and Max Welling. Steerable cnns, 2016.
- [8] Maurice Weiler and Gabriele Cesa. General $e(2)$ -equivariant steerable cnns, 2021.
- [9] Sander Dieleman, Jeffrey De Fauw, and Koray Kavukcuoglu. Exploiting cyclic symmetry in convolutional neural networks, 2016.
- [10] Sander Dieleman, Kyle W. Willett, and Joni Dambre. Rotation-invariant convolutional neural networks for galaxy morphology prediction. *Monthly Notices of the Royal Astronomical Society*, 450(2):1441–1459, apr 2015. doi: 10.1093/mnras/stv632. URL <https://doi.org/10.1093/mnras/stv632>.
- [11] Naveed Akhtar and Ajmal Mian. Threat of adversarial attacks on deep learning in computer vision: A survey. *IEEE Access*, 6:14410–14430, 2018. doi: 10.1109/ACCESS.2018.2807385.
- [12] Jiawei Su, Danilo Vasconcellos Vargas, and Kouichi Sakurai. One pixel attack for fooling deep neural networks. *IEEE Transactions on Evolutionary Computation*, 23(5):828–841, oct 2019. doi: 10.1109/tevc.2019.2890858. URL <https://doi.org/10.1109/tevc.2019.2890858>.
- [13] Xiaoyong Yuan, Pan He, Qile Zhu, and Xiaolin Li. Adversarial examples: Attacks and defenses for deep learning, 2018.
- [14] Aleksander Madry, Aleksandar Makelov, Ludwig Schmidt, Dimitris Tsipras, and Adrian Vladu. Towards deep learning models resistant to adversarial attacks, 2019.
- [15] Weilin Xu, David Evans, and Yanjun Qi. Feature squeezing: Detecting adversarial examples in deep neural networks. In *Proceedings 2018 Network and Distributed System Security Symposium*. Internet Society, 2018. doi: 10.14722/ndss.2018.23198. URL <https://doi.org/10.14722/ndss.2018.23198>.

- [16] Xuanqing Liu, Minhao Cheng, Huan Zhang, and Cho-Jui Hsieh. Towards robust neural networks via random self-ensemble, 2018.
- [17] Beranger Dumont, Simona Maggio, and Pablo Montalvo. Robustness of rotation-equivariant networks to adversarial perturbations, 2018.
- [18] A. Ćiprijanović, D. Kafkes, G. N. Perdue, K. Pedro, G. Snyder, F. J. Sánchez, S. Madireddy, S. M. Wild, and B. Nord. Robustness of deep learning algorithms in astronomy – galaxy morphology studies, 2021. URL <https://arxiv.org/abs/2111.00961>.
- [19] Aleksandra Ćiprijanović, Diana Kafkes, Gregory Snyder, F Javier Sánchez, Gabriel Nathan Perdue, Kevin Pedro, Brian Nord, Sandeep Madireddy, and Stefan M Wild. Deepadversaries: examining the robustness of deep learning models for galaxy morphology classification. *Machine Learning: Science and Technology*, 3(3):035007, 2022.
- [20] Henry W. Leung and Jo Bovy. Deep learning of multi-element abundances from high-resolution spectroscopic data. *mnras*, 483(3):3255–3277, March 2019. doi: 10.1093/mnras/sty3217.
- [21] Chris J. Lintott, Kevin Schawinski, Anže Slosar, Kate Land, Steven Bamford, Daniel Thomas, M. Jordan Raddick, Robert C. Nichol, Alex Szalay, Dan Andreescu, Phil Murray, and Jan Vandenberg. Galaxy zoo: morphologies derived from visual inspection of galaxies from the sloan digital sky survey. *Monthly Notices of the Royal Astronomical Society*, 389(3):1179–1189, sep 2008. doi: 10.1111/j.1365-2966.2008.13689.x. URL <https://doi.org/10.1111/j.1365-2966.2008.13689.x>.
- [22] Chris Lintott, Kevin Schawinski, Steven Bamford, Anže Slosar, Kate Land, Daniel Thomas, Edd Edmondson, Karen Masters, Robert C. Nichol, M. Jordan Raddick, Alex Szalay, Dan Andreescu, Phil Murray, and Jan Vandenberg. Galaxy Zoo 1: data release of morphological classifications for nearly 900 000 galaxies. *mnras*, 410(1):166–178, January 2011. doi: 10.1111/j.1365-2966.2010.17432.x.
- [23] Mike Walmsley, Chris Lintott, Tobias Géron, Sandor Kruk, Coleman Krawczyk, Kyle W. Willett, Steven Bamford, Lee S. Kelvin, Lucy Fortson, Yarin Gal, William Keel, Karen L. Masters, Vihang Mehta, Brooke D. Simmons, Rebecca Smethurst, Lewis Smith, Elisabeth M. Baeten, and Christine Macmillan. Galaxy Zoo DECaLS: Detailed visual morphology measurements from volunteers and deep learning for 314 000 galaxies. *mnras*, 509(3):3966–3988, January 2022. doi: 10.1093/mnras/stab2093.
- [24] Arjun Dey, David J. Schlegel, Dustin Lang, Robert Blum, Kaylan Burleigh, Xiaohui Fan, Joseph R. Findlay, Doug Finkbeiner, David Herrera, Stéphanie Juneau, Martin Landriau, Michael Levi, Ian McGreer, Aaron Meisner, Adam D. Myers, John Moustakas, and Peter et al. Nugent. Overview of the DESI Legacy Imaging Surveys. *aj*, 157(5):168, May 2019. doi: 10.3847/1538-3881/ab089d.
- [25] Gabriele Cesa, Leon Lang, and Maurice Weiler. A program to build E(N)-equivariant steerable CNNs. In *International Conference on Learning Representations*, 2022. URL <https://openreview.net/forum?id=wE4qe9xlnQw>.
- [26] Maurice Weiler and Gabriele Cesa. General E(2)-Equivariant Steerable CNNs. In *Conference on Neural Information Processing Systems (NeurIPS)*, 2019.
- [27] Abien Fred Agarap. Deep learning using rectified linear units (relu), 2019.
- [28] Djork-Arné Clevert, Thomas Unterthiner, and Sepp Hochreiter. Fast and accurate deep network learning by exponential linear units (elus), 2016.
- [29] Nitish Srivastava, Geoffrey Hinton, Alex Krizhevsky, Ilya Sutskever, and Ruslan Salakhutdinov. Dropout: A simple way to prevent neural networks from overfitting. *Journal of Machine Learning Research*, 15(56):1929–1958, 2014. URL <http://jmlr.org/papers/v15/srivastava14a.html>.
- [30] Kaiming He, Xiangyu Zhang, Shaoqing Ren, and Jian Sun. Deep residual learning for image recognition, 2015.

- [31] Adam Paszke, Sam Gross, Francisco Massa, Adam Lerer, James Bradbury, Gregory Chanan, Trevor Killeen, Zeming Lin, Natalia Gimelshein, Luca Antiga, Alban Desmaison, Andreas Kopf, Edward Yang, Zachary DeVito, Martin Raison, Alykhan Tejani, Sasank Chilamkurthy, Benoit Steiner, Lu Fang, Junjie Bai, and Soumith Chintala. Pytorch: An imperative style, high-performance deep learning library. In *Advances in Neural Information Processing Systems 32*, pages 8024–8035. Curran Associates, Inc., 2019. URL <http://papers.neurips.cc/paper/9015-pytorch-an-imperative-style-high-performance-deep-learning-library.pdf>.
- [32] Daniel Franzen and Michael Wand. Nonlinearities in steerable $so(2)$ -equivariant cnns, 2021.
- [33] Ilya Loshchilov and Frank Hutter. Decoupled weight decay regularization, 2019.
- [34] Rui Wang, Robin Walters, and Rose Yu. Approximately equivariant networks for imperfectly symmetric dynamics, 2022.
- [35] Marc Finzi, Gregory Benton, and Andrew Gordon Wilson. Residual pathway priors for soft equivariance constraints, 2021.
- [36] Sandesh Kamath, Amit Deshpande, Subrahmanyam Kambhampati Venkata, and Vineeth N Balasubramanian. Can we have it all? on the trade-off between spatial and adversarial robustness of neural networks. In M. Ranzato, A. Beygelzimer, Y. Dauphin, P.S. Liang, and J. Wortman Vaughan, editors, *Advances in Neural Information Processing Systems*, volume 34, pages 27462–27474. Curran Associates, Inc., 2021. URL https://proceedings.neurips.cc/paper_files/paper/2021/file/e6ff107459d435e38b54ad4c06202c33-Paper.pdf.
- [37] Laurens van der Maaten and Geoffrey Hinton. Visualizing data using t-sne. *Journal of Machine Learning Research*, 9(86):2579–2605, 2008. URL <http://jmlr.org/papers/v9/vandermaaten08a.html>.
- [38] Željko et al. Ivezić. LSST: From Science Drivers to Reference Design and Anticipated Data Products. *apj*, 873(2):111, March 2019. doi: 10.3847/1538-4357/ab042c.

7 Appendix

Layers	Properties	Stride	Padding	Output Shape
Input	3 x 255 x 255			
Conv2D (w/ BatchNorm2D)	Filters: 12 Kernel: 3x3 Activation: ReLU	2	2	(12, 129, 129)
Conv2D (w/ BatchNorm2D)	Filters: 24 Kernel: 3x3 Activation: ReLU	1	1	(24, 129, 129)
MaxPool2D	Kernel: 2	2	0	(24, 64, 64)
Conv2D (w/ BatchNorm2D)	Filters: 48 Kernel: 3x3 Activation: ReLU	1	1	(48, 64, 64)
Conv2D (w/ BatchNorm2D)	Filters: 48 Kernel: 3x3 Activation: ReLU	1	1	(48, 64, 64)
MaxPool2D	Kernel: 2	2	0	(48, 32, 32)
Conv2D (w/ BatchNorm2D)	Filters: 48 Kernel: 3x3 Activation: ReLU	1	1	(48, 32, 32)
Conv2D (w/ BatchNorm2D)	Filters: 48 Kernel: 3x3 Activation: ReLU	1	1	(48, 32, 32)
Conv2D (w/ BatchNorm2D)	Filters: 96 Kernel: 3x3 Activation: ReLU	1	1	(96, 32, 32)
MaxPool2D	Kernel: 2	2	0	(96, 16, 16)
Conv2D (w/ BatchNorm2D)	Filters: 96 Kernel: 3x3 Activation: ReLU	1	1	(96, 16, 16)
Conv2D (w/ BatchNorm2D)	Filters: 96 Kernel: 3x3 Activation: ReLU	1	1	(96, 16, 16)
MaxPool2D	Kernel: 2	2	0	(96, 8, 8)
Conv2D (w/ BatchNorm2D)	Filters: 112 Kernel: 3x3 Activation: ReLU	1	1	(112, 8, 8)
Conv2D (w/ BatchNorm2D)	Filters: 192 Kernel: 3x3 Activation: ReLU	1	1	(192, 8, 8)
MaxPool2D	Kernel: 2	2	0	(192, 4, 4)
Linear (w/ BatchNorm1D)	Input Dimension: 3072 Output Dimension: 64 Activation: ELU			(, 64)
Linear (w/ BatchNorm1D)	Input Dimension: 64 Output Dimension: 32 Activation: ELU			(, 32)
Linear:	Input Dimension: 32 Output Dimension: 10 Activation: None			(, 10)

Table 1: Architecture of CNN baseline.

Layers	Properties	Stride	Padding	Output Shape
Input	3 x 255 x 255			
MaskModule	Margin: 1 Sigma: 2.0			(3 x 255 x 255)
R2Conv (w/ InnerBatchNorm)	Filters: 12 Kernel: 3x3 Activation: ReLU	2	2	($N * 12, 129, 129$)
R2Conv (w/ InnerBatchNorm)	Filters: 24 Kernel: 3x3 Activation: ReLU	1	1	($N * 24, 129, 129$)
PointwiseAvgPoolAntialiased	Sigma: 0.66	2	0	($N * 24, 65, 65$)
R2Conv (w/ InnerBatchNorm)	Filters: 48 Kernel: 3x3 Activation: ReLU	1	1	($N * 48, 65, 65$)
R2Conv (w/ InnerBatchNorm)	Filters: 48 Kernel: 3x3 Activation: ReLU	1	1	($N * 48, 65, 65$)
PointwiseAvgPoolAntialiased	Sigma: 0.66	2	0	($N * 48, 33, 33$)
R2Conv (w/ InnerBatchNorm)	Filters: 48 Kernel: 3x3 Activation: ReLU	1	1	($N * 48, 33, 33$)
R2Conv (w/ InnerBatchNorm)	Filters: 48 Kernel: 3x3 Activation: ReLU	1	1	($N * 48, 33, 33$)
R2Conv (w/ InnerBatchNorm)	Filters: 96 Kernel: 3x3 Activation: ReLU	1	1	($N * 96, 33, 33$)
PointwiseAvgPoolAntialiased	Sigma: 0.66	2	0	($N * 96, 17, 17$)
R2Conv (w/ InnerBatchNorm)	Filters: 96 Kernel: 3x3 Activation: ReLU	1	1	($N * 96, 17, 17$)
R2Conv (w/ InnerBatchNorm)	Filters: 96 Kernel: 3x3 Activation: ReLU	1	1	($N * 96, 17, 17$)
PointwiseAvgPoolAntialiased	Sigma: 0.66	2	0	($N * 96, 9, 9$)
R2Conv (w/ InnerBatchNorm)	Filters: 112 Kernel: 3x3 Activation: ReLU	1	1	($N * 112, 9, 9$)
R2Conv (w/ InnerBatchNorm)	Filters: 192 Kernel: 3x3 Activation: ReLU	1	1	($N * 192, 9, 9$)
PointwiseAvgPoolAntialiased	Sigma: 0.66	2	0	($N * 192, 5, 5$)
GroupPooling				(192, 5, 5)
Linear (w/ BatchNorm1D)	Input Dimension: 4800 Output Dimension: 64 Activation: ELU			(, 64)
Linear (w/ BatchNorm1D)	Input Dimension: 64 Output Dimension: 32 Activation: ELU			(, 32)
Linear:	Input Dimension: 32 Output Dimension: 10 Activation: None			(, 10)

Table 2: Architecture of GCNNs. In constructing GCNNs equivariant to C_N , N in the output shape is exactly equal to the group order. For GCNNs equivariant to D_N , let $N \rightarrow 2N$.